

Characteristic of alumina-based microfiltration ceramic membrane

Hyunsoo Kim¹, Oyunbileg Purev¹, Eunji Myung², Kanghee Cho^{*3} and Nagchoul Choi^{**3}

¹Department of Energy and Resource Engineering, Chosun University, Gwangju 61452, Korea

²Green-bio Research Facility Center, Seoul National University, Gangwon-do 25354, Korea

³Research Institute of Agriculture and Life Sciences, Seoul National University, Seoul 08826, Korea

(Received September 13, 2022, Revised January 1, 2023, Accepted January 3, 2023)

Abstract. This work addresses the development of microfiltration ceramic membrane from alumina using extrusion method. The membranes were sintered at different temperatures ranging between 1000 and 1300°C. The alumina was characterized with thermogravimetric analysis, particle size distribution, X-ray diffraction, Fourier transform infrared spectrometer and scanning electron microscope analysis. Subsequently, the effect of sintering temperature on the membrane properties such as porosity, flexural strength, and pure water permeability was investigated and optimized for the sintering temperature. It is observed that with increasing sintering temperature, the porosity of the membranes decreases and the flexural strength, and pure water permeability of the membranes increase. The uncoated and coated membranes were compared at constant flux mode of filtration. Under the turbidity solution recirculation alone at 100 NTU, trans-membrane pressure (TMP) of uncoated membrane remained constant when the filtration flux was below 121 Lm² h⁻¹, while the coated membrane was 111 Lm² h⁻¹. Although suction pressure increased more rapidly at higher turbidity, coated membrane filtration showed better removal efficiency of the turbidity.

Keywords: alumina; ceramic membrane; fouling; microfiltration; turbidity

1. Introduction

The industrial wastewater contains high concentration of hazardous matters. The discharge of wastewater containing organic and particulate materials can cause serious environmental hazard and esthetic pollution (Chang *et al.* 2020). In wastewater treatment, high-turbidity is one of the main problems, the treatment cost increases and the coagulation efficiency decreases. Thus, the treatment technique efficiency decreases due to the presence of colloidal materials such as organic, inorganic and biological contaminants. For these environmental problems, membrane technology is one of the most popular methods for wastewater treatment due to its advantages of simple operation, and high efficiency (He *et al.* 2019, Eray *et al.* 2021).

Currently, membranes can be made with a wide variety of materials and methods of manufacture (Samaei *et al.* 2018, Wang *et al.* 2020). Ceramics and polymers are two main materials used for membrane fabrication. Among them, ceramic membrane have been the subject of attention, as researchers have endeavored to exploit their unique properties, such as mechanical and chemical stability, and thermal stresses (Song *et al.* 2017). In particular, ceramic membranes are among the most promising application of low-pressure membrane filtration such as microfiltration,

and have advantages of high filtration flux, long service life as well as easy cleaning (Aziz *et al.* 2019, Le *et al.* 2019). Among the low pressure membrane processes, microfiltration is the most useful method for turbidity wastewater treatment. In recent decades, ceramic microfiltration is one of the most popular methods for wastewater treatment containing organic and inorganic pollutants (e.g. suspended solids, colloids, pathogens). In addition, microfiltration is environmental friendly separation technique that is suitable to solve many environmental issues at low cost (Arzani *et al.* 2018, Ha *et al.* 2016).

Despite the increasing applications of ceramic membranes in wastewater treatment, their production cost is expensive due to fabrication process followed by shaping and high sintering temperature. To address these problems, the cost of ceramic membrane could be reduced by using low cost materials and the development of cheaper fabrication techniques. However, inorganic materials used for ceramic membrane fabrication are critical in determining function and performance. Therefore, the selection criteria of ceramic materials are not random, but according to their physical and chemical properties, and other beneficial feature for wastewater treatment (Qin *et al.* 2020, Liang *et al.* 2021). Among various inorganic membrane materials, oxide of alumina, silica, zirconia, and titanium have been commercialized and applied for membrane manufacturing (Lu *et al.* 2019, Saja *et al.* 2018, Hubadillah *et al.* 2018). However, manufacturing and applications of these inorganic materials are still challenging. In addition, the design of membrane modules and optimization of operating conditions is also a factor to be considered. Therefore, the focus of future research should be in the development of the control of the average

*Corresponding author, Ph.D.,
E-mail: kanghee1226@snu.ac.kr

**Co-corresponding author, Ph.D.,
E-mail: nagchoul@snu.ac.kr

pore size, the flexural strength, and water permeability of the ceramic membranes. In this study, the alumina was selected because of its exceptional characteristics such as crystallinity, high purity and thermal stability. The objective of this article is to study the influence of sintering temperature on the properties of alumina-based ceramic microfiltration membrane evaluate its separation performance for the treatment of turbidity solution of organic substances.

2. Materials and methods

2.1 Materials

Alumina (AP 400, POS-HIAL, Korea) was used for the preparation of the ceramic support layer. The alumina powder is mainly composed of Al_2O_3 (98.99%). The median particle size (D50) of the alumina was 0.7 μm . To supplement clay (GF-1250, Duckyu, Korea), silica (KS-1500, 21centurysilica, Korea), and feldspar (F-S, BMS, Korea) were also used. Methyl-cellulose was obtained from LOTTE Fine Chemical Co., Ltd., Korea. Isopropyl alcohol (IPA) was procured from Samchun Pure Chemical Co., Ltd., Korea. Glycerol was procured from the Sigma-Aldrich, USA. All solutions were prepared using deionized (DI) water. To apply the coating layers on the alumina support layers, alumina (AES-11) with a median particle size (D50) of 0.43 μm was procured from the Sumitomo Chemical Co., Ltd., Japan. Polyacrylic acid-based copolymers as a binder (AP-2) was obtained from Yuken Industry Co., Ltd., Japan. Darvan-CN as a dispersing agent was obtained from the R.T. Vanderbilt Holding Co., USA. Hydrazine sulfate ($\text{N}_2\text{H}_6\text{SO}_4$, Duksan, Korea) and hexamethylenetetramine ($\text{C}_6\text{H}_{12}\text{N}_4$, Samchun, Korea) were used for the preparation of turbidity solution.

2.2 Characterization of alumina

The thermo-gravimetric behavior of alumina powder (AP 400) was analyzed with a thermo-gravimetric analyzer (TGA, SDT Q600, TA Instruments, USA) under air environment. The AP 400 was analyzed at a heating rate of 10 $^\circ\text{C}/\text{min}$ under air, and the scan range was from approximately 1300 $^\circ\text{C}$. A series of 10 g samples were taken in pre-weighed quartz boat, pyrolyzed in electric furnace under air atmosphere at different temperatures (1100, 1200, and 1300 $^\circ\text{C}$), a heating rate of 10 $^\circ\text{C}/\text{min}$ was performed for electric furnace to reach the specific temperature and residence times (60 min). Mineral phases in the sintering samples were identified using XRD (X'Pert Pro MRD, PANalytical, The Netherlands). The average particle sizes of the sample was determined using a particle size analyzer (Mastersizer 2000, Malvern Panalytical Ltd., UK).

2.3 Preparation of ceramic membrane

2.3.1 Alumina-based ceramic support layer

Based on the Alumina-based ceramic support layer, the inorganic raw materials was prepared following procedures

modified from Ha *et al* (2016). Alumina (AP 400), clay, silica and feldspar were used for the preparation of the alumina support layer. The different kinds of dry powder (clay, silica and feldspar; 3wt.%, respectively) were added into a powder mixer (Pk-50, Kikusui, Japan) containing 70 wt.% of alumina and mixed for 1 h. A mixture of 6 wt.% of methyl-cellulose, 2 wt.% of glycerol and 12 wt.% of distilled water was stirred at room temperature for 1 h. Then, the resultant slurry as a binder was added into a ribbon mixer (mixer, Techinkorea, Korea) containing mixed powders and mixed for 1 h. The homogeneous mixture was aged for 24h at room temperature and extruded using a double screw extruder (H30-2, Dongkwangtech, Korea). The extruded alumina composite support layer as specimen had flat-tubular. The flat tube-type dimensions of the extruded support were, a width of 75 mm, a length of 250 mm and a height of 4 mm, with 16 inner holes (2 mm wide and 2 mm high). After extrusion, the specimen was dried in an oven at 65 $^\circ\text{C}$ overnight. Then, heat treated at 400 $^\circ\text{C}$ for 1 h to burn off the binder, and sintered at 1100 $^\circ\text{C}$ to 1300 $^\circ\text{C}$ for 1 h.

2.3.2 Coating of the alumina active layers on support membranes

The dip-coating method was used to prepare an alumina active layer over the flat-tubular alumina support. For the preparation of the alumina coating solution, alumina powder (AES-11, 8 wt.%), AP-2 (2 wt.%), IPA (33 wt.%), and DI (57 wt.%) were added into plastic bottles containing alumina balls (3 mm in diameter). 0.2 wt.% of Darvan-CN was added as a dispersant, and the solution was ball-milled at 200 rpm for 12 h. The slurries were mixed in a ball mill for 12h to ensure dispersion of the alumina particles.

The average particle sizes of the alumina coating slurry was determined using a particle size analyzer. The median particle size (D50) of the alumina was 0.3 μm . For coating, the inner holes were first sealed by masking tape, in order to coat only outside surface. The alumina support layers were dip-coated at a descending speed of 1.1 cm/s, maintained for 1 min, before being retracted at a withdrawal speed of 0.5 cm/s, and dried at room temperature for 24h, before being heat treated from 1200 $^\circ\text{C}$ for 1h.

2.4 Characterization of MF ceramic membranes

The flexural strength of sintered specimens was determined by using a three points bending apparatus with a constant displacement rate of about 0.2 mm/min, using a universal mechanical testing machine (DTU-900, Daekyung, Korea). The surface morphology and crosssectional morphologies of the ceramic membranes for both support and coated layer were examined via field-emission scanning electron microscopy (FE-SEM) analysis. The pore size distribution and mean pore size of the ceramic membranes before and after alumina coating were analyzed using a mercury porosimetry analysis technique (AutoPore IV 9500, Micromeritics, USA) which is based on the intrusion of mercury into a porous structure under stringently controlled pressures. Water permeability of the ceramic membranes were determined by passing deionized water through the membrane under different flow rates.

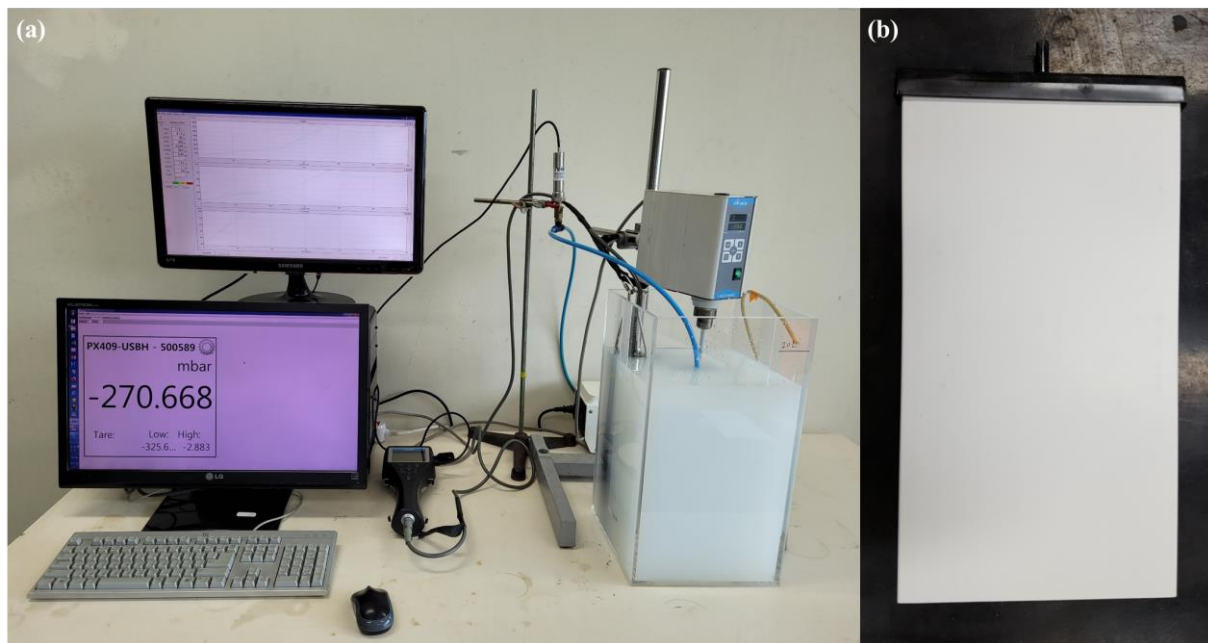


Fig. 1 (a) The digital photographs of submerged ceramic membrane reactor; and (b) the digital photographs of flat ceramic membrane

2.5 Experimental design

Hydrazine sulfate and hexamethylenetetramine were used to prepare the turbidity solution of organic substances. The turbidity solution was prepared following procedures (Su *et al.* 2020). 5.0 g of hydrazine sulfate dissolved in deionized water to a volume of 400 mL. Then, 50 g of hexamethylenetetramine was dissolved in deionized water to a volume of 400 mL. Mix the two solutions and add deionized water until the total solution volume is 1000 mL, and mixed well. The mixture was allowed to react without stirring for 48 h at 25 °C. The turbidity of this turbidity solution was 4000 NTU. The turbidity solution was diluted for the preparation of turbidity solutions.

A simple schematic of the ceramic membrane experimental setup is illustrated in Fig. 1. A flat-tubular, ceramic membrane was submerged into the reactor and operated at constant flux of $70 \text{ Lm}^{-2}\text{h}^{-1}$. The reactor had 20 L of effective volume. Trans-membrane pressure (TMP) was recorded by a digital pressure gauge (PX409-015GUSBH, Omega Engineering Inc., USA), connected between the membranes and the peristaltic permeate pumps (BT100-2J, Longer Pump, China). Permeate was produced by using peristaltic pump constantly and suction pressure with time was monitored as an indicator of membrane fouling. A permeate produced by the ceramic membrane was returned to the turbidity solution to maintain water level constantly. The fouling propensity during turbidity treatment was compared between uncoated and alumina-coated ceramic membranes. Samples of membrane feed water and permeate were taken to measure the turbidity. Turbidity was determined by using a multi-parameter probe (U-50, HORIBA, Japan). The turbidity data was collected every 1 min using a data acquisition software.

3. Results and discussion

3.1 Characterization of alumina

The mineral found by the XRD analysis of alumina powder was $\alpha\text{-Al}_2\text{O}_3$. The TG and DSC curves of the alumina at a heating rate of $10 \text{ }^\circ\text{C}/\text{min}$ in air are shown in Fig. 2. The DTA curve was divided into three stages for the sintered process. The alumina showed weight loss during the before 200 °C because of the evaporation of moisture and the exothermic peak corresponds to the loss of absorbed water (Aziz *et al.* 2019). The second temperature interval occurs in 200 to 500 °C region resulting in 0.91% mass loss owing to the decomposition of organics. In contrast, it is apparent that there is a substantial weight increment after heating at a temperature of more than 500 °C. The main increase in weight of the alumina powder is attributed to the oxidation in the atmospheric air, which may be related to the endothermic peak. Such result indicated that the increase in sintering temperature encourages the crystal growth (Lu *et al.* 2019).

To study the phase transformation of roasted alumina, XRD analyses were conducted to confirm the changes. The XRD peak of the roasted alumina did not show any distinct change from the XRD pattern of the original alumina (Fig. 3). However, the average particle size (D50) of alumina from 4.58 to $5.80 \text{ }\mu\text{m}$ from 1100 to 1300 °C (Table 1). It can be seen that the sintering temperature affects the morphology of alumina significantly. The increased sintering temperature of alumina may result in the change of the membrane properties such as porosity, surface area, pore size and morphology in the as-made alumina membrane. Temperature was found to be critical for crystal growth in ceramic studies (Hai *et al.* 2020). He *et al.* (2020) reported that the increased sintering temperature facilitated

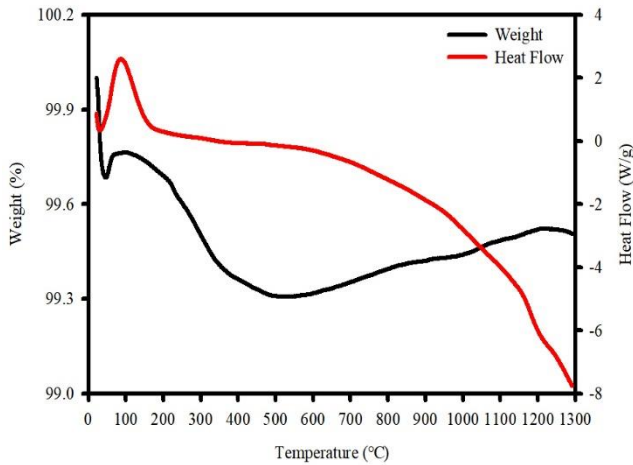


Fig. 2 Thermal analysis of alumina

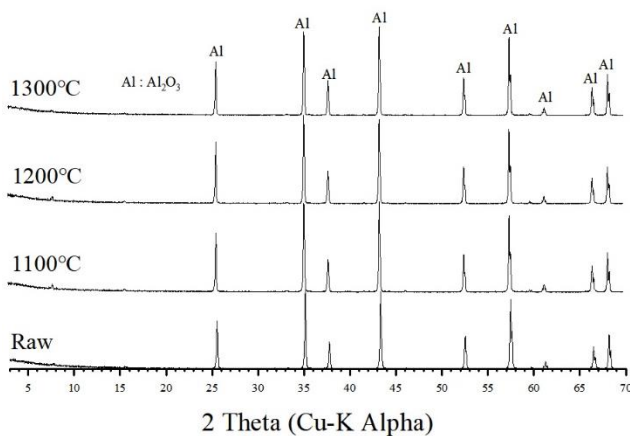


Fig. 3 XRD patterns of alumina after sintering at 1100 to 1300 °C

mass transfer mechanisms, like grain boundary diffusion and lattice diffusion.

Under SEM analysis, the crystal growth of alumina in the different temperature sintering was observed. The alumina prepared at temperatures of 1000 to 1300 °C was shown in Fig. 4. It can be seen that particles in the sintering at 1300 °C is larger than in the sintering at 1000 °C. When the temperature increased from 1000 to 1300 °C, the surface was relatively dense consisting of coarse particles. The results indicated that higher temperature treatment can lead to the decrease of surface area in alumina, which further led to the lower porosity in the as-made alumina support layer.

3.2 The characteristics of ceramic membranes

3.2.1 The characteristics of alumina-based support layer

The effect of the sintering temperatures on the support layer surface was investigated. The alumina-based support membranes fabricated were sintered at 1100, 1200, and 1300 °C for 1 h. When the temperature increased from 1100 to 1300 °C, most prominent feature of the ceramic membranes was in the smoothness of their surfaces. In this

Table 1 Variation of specific surface area with sintering temperature

	Specific Surface Area (m ² /kg)	Dv (10) μm	Dv (50) μm	Dv (90) μm
Raw	10870	0.212	0.788	11.4
1100°C	9673	0.206	4.58	26.4
1200°C	8792	0.217	5.46	28.2
1300°C	8858	0.211	5.80	141

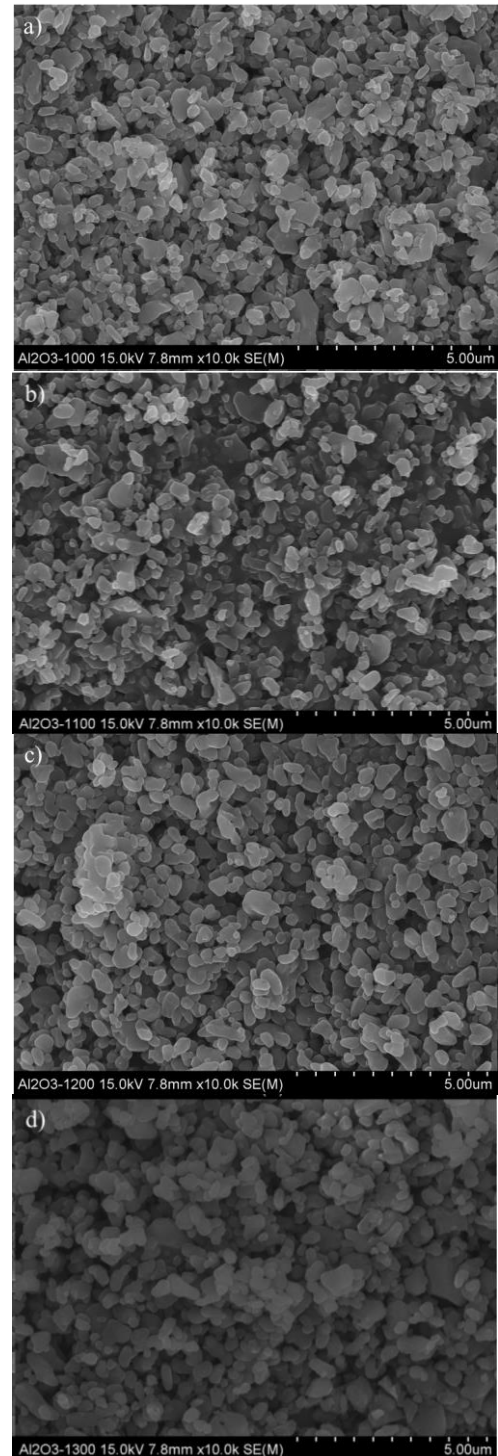


Fig. 4 The morphology of alumina obtained at temperature ranged from 1000 to 1300 °C

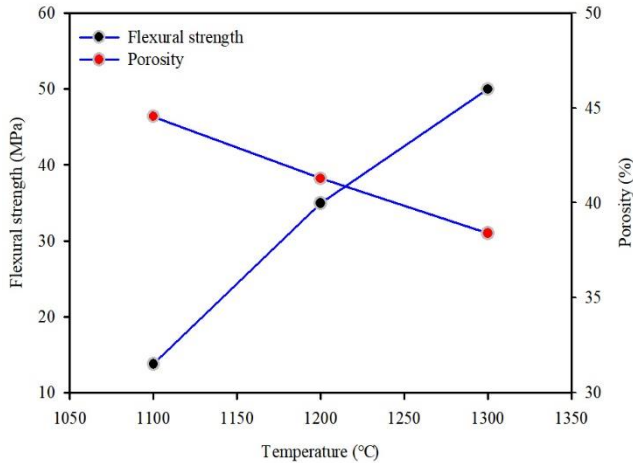


Fig. 5 Characteristics of alumina-based support membranes sintering at different temperature for 1 h (The experiments were performed in triplicate and the standard deviation of the results was estimated in the order of + 2%)

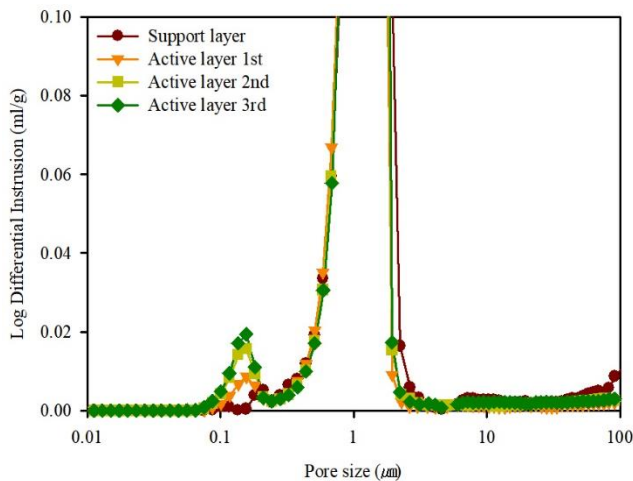


Fig. 6 Pore-size distribution of the alumina-based support membranes and varying the number of coating layers

study, average pore sizes ranged from 0.05 to 1.24 μm , which is similar to the pore size of alumina made by Song *et al.* (2017), and thus, the support layers, even without the coating of separation layer, may be used for microfiltration membranes. In also, these indicate that porosity depends more on sintering temperature than the particle size of raw powder. When the support layer was sintered at 1100 $^{\circ}\text{C}$, flexural strength decreased to be around 13.7 MPa. As expected, the samples with high porosity presented the low flexural strength. With temperature elevated from 1100 to 1300 $^{\circ}\text{C}$, the observed flexural strength of as made alumina support layer was increased (Fig. 5). Generally, the support layer must be of the mechanical strength in order to have a water transport resistance or other factors such as chemical resistance and durability. As a result, support layer sintered at 1100 $^{\circ}\text{C}$ have disadvantages including low mechanical strength. The porosity of the support layer must also be considered, thus the alumina-based support layer was sintered at 1200 $^{\circ}\text{C}$ for 1 h.

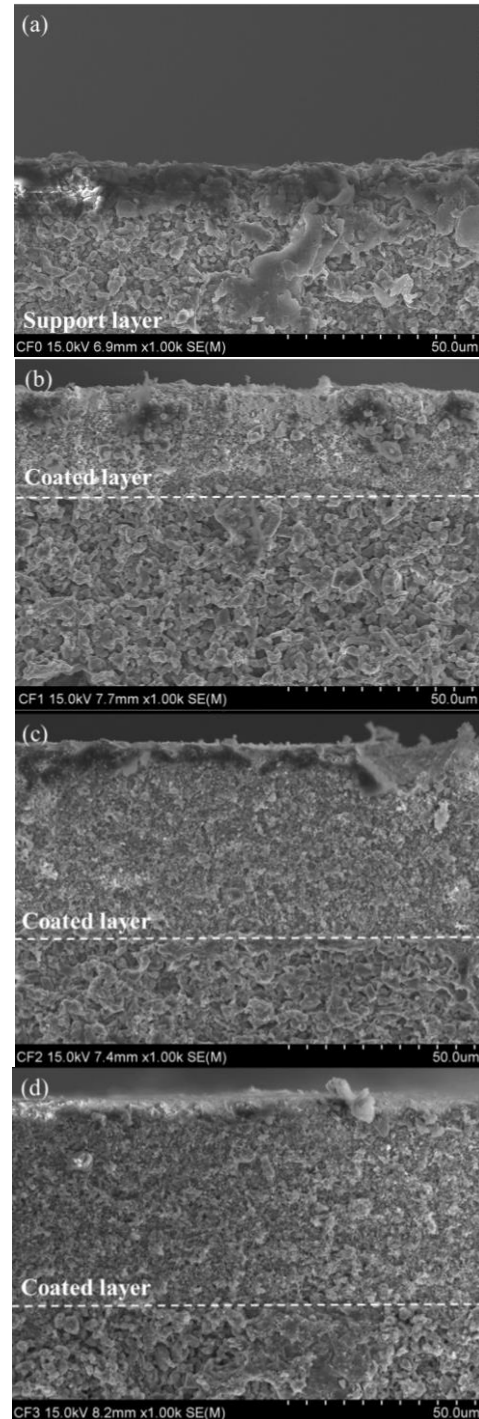


Fig. 7 SEM images of the cross-section of alumina-based ceramic membrane, (a) support layer, (b) coated one times (c) coated two time (d) coated three time

3.2.2 The effect of the coating process on the ceramic membrane

The effect of the coating process on the ceramic membrane was investigated. The coating solution was prepared as alumina with an average particles size (D50) of 0.4 μm in order to coat separation layer onto a support layer through dip-coating process. The holding time during coating through dip-coating in the coating process was

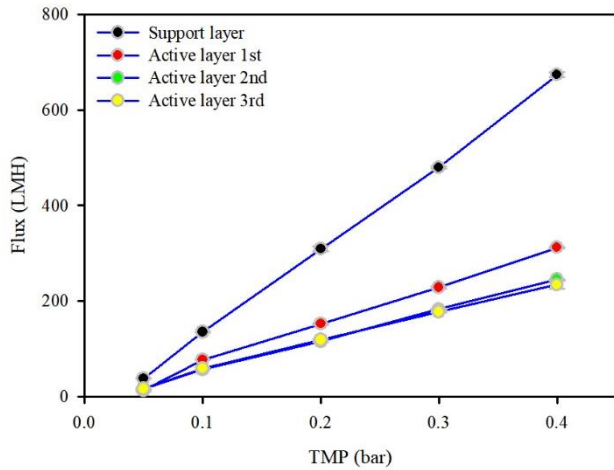


Fig. 8 The water permeability of alumina support layer and alumina-coated alumina ceramic membrane

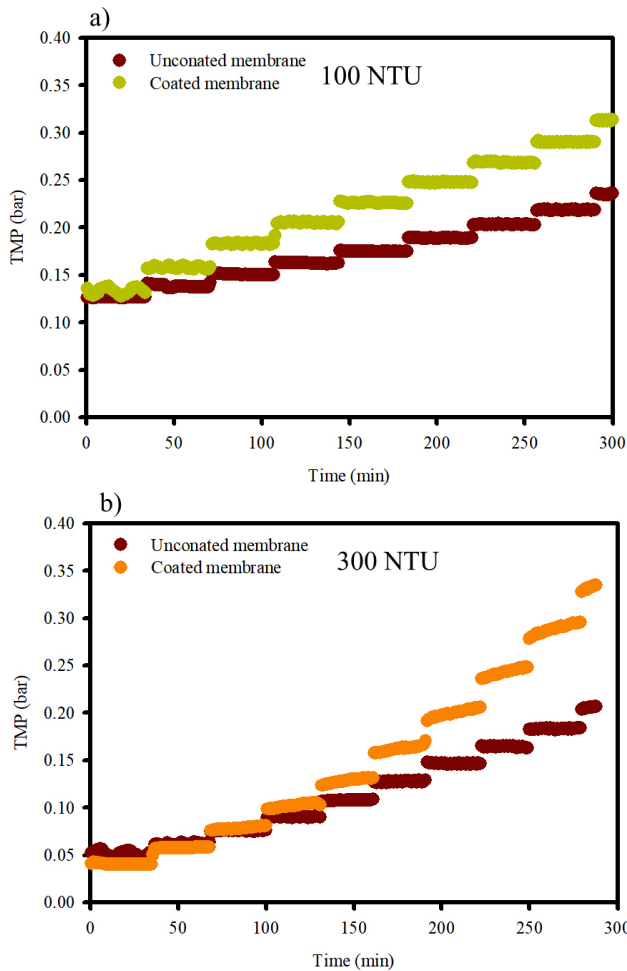


Fig. 9 Critical flux measurement of alumina support layer and alumina-coated alumina ceramic membrane with time course for the TMP changes in a stepwise increased membrane flux

controlled at 1 min, which were coated and then sintered at 1200 °C for 1h. The average pore size of the alumina support layer is about 1.24 μm . After coating with the alumina, the average pore sizes of the coating layers were

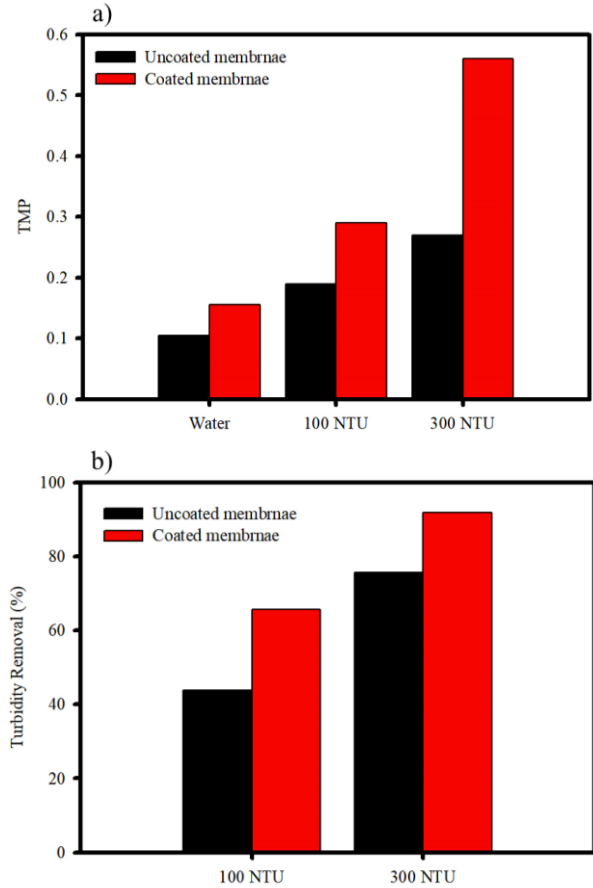


Fig. 10 (a) Ceramic membrane fouling tendency and (b) turbidity removal by uncoated membrane and coated membrane

found to be between 1.09 to 1.04 μm (Fig. 6).

The cross-section of coated alumina membrane was compared with that of uncoated support layer, as shown in Fig. 7. The SEM images show that the homogenous section morphology indicating dense fragments, and defect-free membrane with uniformly distributed pores was obtained. Furthermore, the membrane showed that alumina coating layer was well distributed with about $\sim 53 \mu\text{m}$ thickness in the absence of significant defects and delamination between coating and alumina based support layers.

3.3 The characteristics of ceramic membrane on critical flux

The pure water permeability are presented in Fig. 8 to compare the effects of coating layer by membranes in the coating process. The pure water permeability of uncoated membrane was $673 \text{ Lm}^{-2} \text{ h}^{-1} \text{ bar}^{-1}$ but it was decreased to $234 \text{ Lm}^{-2} \text{ h}^{-1} \text{ bar}^{-1}$ for coated membrane (pore size 1.04 μm , coated three time). As the pore size decreased from 1.24 to 1.04 μm , the relative permeability rate tended to decrease from 53.7 to 65.3%. This correlates with the water permeability curves of typical microfiltration membranes (Ha *et al.* 2017). Therefore, the water permeability of the support decreased after being deposition with an alumina coating layer.

Variations of TMP of uncoated and coated membranes corresponding to the 100 and 300 NTU in the turbidity solution during the measurement of critical flux are shown in Fig. 9. The pH of the turbidity solution for uncoated and coated membrane filtration was kept stable at 6.0 to avoid any effect of zeta potential. Under the turbidity solution recirculation alone at 100 NTU, TMP of uncoated membrane remained constant when the filtration flux was below $121 \text{ Lm}^{-2} \text{ h}^{-1}$, while the coated membrane was $111 \text{ Lm}^{-2} \text{ h}^{-1}$. However, the critical flux above which TMP starts increasing was observed as $76 \text{ Lm}^{-2} \text{ h}^{-1}$ at 300 NTU with coated membrane. The membrane fouling increased with flux, which suggests the advantage of operating at lower fluxes in order to avoid frequent backwashing and decrease membrane fouling rates.

Fig. 10 shows turbidity removal efficiency for uncoated membrane and coated membrane. When operating at constant flux, membrane fouling leads to TMP increase, the turbidity removal efficiency increased. Although suction pressure increased more rapidly at higher turbidity, coated membrane filtration showed better removal efficiency of the turbidity. Higher turbidity removal with coated membrane be caused by the coating layer with smaller surface pore size than the one of uncoated membrane. In addition, these results indicate the presence of cake layer on membrane surface acted as secondary membrane for the rejection of turbidity, which is consistent with TMP as shown in Fig. 10 (a).

4. Conclusions

This study focuses on the influence of sintering temperature on the properties of alumina-based ceramic microfiltration membrane evaluated its separation performance for the treatment of turbidity solution of organic substances. Alumina based ceramic microfiltration membrane was prepared by sintering temperature ranged from 1000 to 1300 °C. It can be seen that the sintering temperature affects the crystal growth of alumina significantly. The results indicated that properties (i.e. porosity, pore size, flexural strength) of alumina membrane were greatly influenced by the sintering at different temperatures. Higher turbidity removal with coated membrane be caused by the coating layer with smaller surface pore size than the one of uncoated membrane.

Acknowledgments

This study was supported by Korea Environmental Industry & Technology Institute (Grant numbers 2020002870001).

References

Arzani, M., Mahdavi, H.R., Sheikhi, M., Mohammadi, T., Bakhtiari, O. (2018), "Ceramic monolith as microfiltration membrane: Preparation, characterization and performance evaluation", *Appl. Clay Sci.*, **161**, 456-463.

<https://doi.org/10.1016/j.clay.2018.05.021>.

Aziz, M.H.A., Othman, M.H.D., Hashim, N.A., Rahman, M.A., Jaafar, J., Hubadillah, S.K., Tai, Z.S. (2019), "Pretreated aluminium dross waste as a source of inexpensive alumina-spinel composite ceramic hollow fibre membrane for pretreatment of oily saline produced water", *Ceram. Int.*, **45**(2), 2069-2078. <https://doi.org/10.1016/j.ceramint.2018.10.110>.

Chang, S., Ahmad, R., Kwon, D.E., Kim, J. (2020), "Hybrid ceramic membrane reactor combined with fluidized adsorbents and scouring agents for hazardous metal-plating wastewater treatment", *J. Hazard Mater.*, **388**, 121777. <https://doi.org/10.1016/j.jhazmat.2019.121777>.

Eray, E., Candelario, V.M., Boffa, V., Safafar, H., Østedgaard-Munck, D.N., Zahrtmann, N., Kadrispahic, H., Jørgensen, M.K. (2021), "A roadmap for the development and applications of silicon carbide membranes for liquid filtration: Recent advancements, challenges, and perspectives", *Chem. Eng. J.*, **414**, 128826. <https://doi.org/10.1016/j.cej.2021.128826>.

Ha, J.H., Abbas Bukhari, S.Z., Lee, J., Song, I.H., Park, C. (2016), "Preparation processes and characterizations of alumina-coated alumina support layers and alumina-coated natural material-based support layers for microfiltration", *Ceram. Int.*, **42**(12), 13796-13804. <https://doi.org/10.1016/j.ceramint.2016.05.181>.

Ha, J.H., Lee, S., Bukhari, S.Z.A., Choi, J.R., Lee, J., Song, I.H., Lee, S.J., Choi, J. (2017), "Preparation and characterization of alumina-coated silicon carbide supports", *Ceram. Int.*, **43**(12), 9481-9487. <https://doi.org/10.1016/j.ceramint.2017.04.126>.

Hai, C., Zhang, G., Liu, J., Zhou, Y., Dong, S., Zeng, J., Li, X., Sun, Y., Shen, Y. (2020), "ζ-potential variations of micro-nano sized hexagram-like $\alpha\text{-Al}_2\text{O}_3$ particles", *J. Nanopart. Res.*, **22**(3), 1-12. <https://doi.org/10.1007/s11051-020-04786-x>

He, Z., Lyu, Z., Gu, Q., Zhang, L., Wang, J. (2019), "Ceramic-based membranes for water and wastewater treatment", *Colloids Surf. A*, **578**. <https://doi.org/10.1016/j.colsurfa.2019.05.074>.

He, Z., Ng, T.C.A., Lyu, Z., Gu, Q., Zhang, L., Ng, H.Y., Wang, J. (2020), "Alumina double-layered ultrafiltration membranes with enhanced water flux", *Colloids Surf. A*, **587**.

Hubadillah, S.K., Othman, M.H.D., Matsuura, T., Ismail, A.F., Rahman, M.A., Harun, Z., Jaafar, J., Nomura, M. (2018), "Fabrications and applications of low cost ceramic membrane from kaolin: A comprehensive review", *Ceram. Int.* **44**(5), 4538-4560. <https://doi.org/10.1016/j.ceramint.2017.12.215>.

Le, M.H., Kim, K.J., Jeong, S., Jang, A. (2019), "Effect of charged nano-particles on ceramic microfiltration membrane fouling", *J. Ind. Eng. Chem.*, **72**, 125-132. <https://doi.org/10.1016/j.jiec.2018.12.012>.

Liang, D., Huang, J., Zhang, H., Fu, H., Zhang, Y., Chen, H. (2021), "Influencing factors on the performance of tubular ceramic membrane supports prepared by extrusion", *Ceram. Int.*, **47**(8), 10464-10477. <https://doi.org/10.1016/j.ceramint.2020.12.235>.

Lu, X., Yang, J., Li, X., Sun, F., Wang, F., Chao, Y. (2019), "Effects of phase transformation on properties of alumina ceramic membrane: A new assessment based on quantitative X-ray diffraction (QXRD)", *Chem. Eng. Sci.*, **199**, 349-358. <https://doi.org/10.1016/j.ces.2018.12.054>.

Qin, H., Guo, W., Gao, P., Xiao, H. (2020), "Spheroidization of low-cost alumina powders for the preparation of high-flux flat-sheet ceramic membranes", *Ceram. Int.*, **46**(9), 13189-13197. <https://doi.org/10.1016/j.ceramint.2020.02.093>.

Saja, S., Bouazizi, A., Achiou, B., Ouammou, M., Albizane, A., Bennazha, J., Younssi, S.A. (2018), "Elaboration and characterization of low-cost ceramic membrane made from natural Moroccan perlite for treatment of industrial wastewater", *J. Environ. Chem. Eng.*, **6**(1), 451-458. <https://doi.org/10.1016/j.jece.2017.12.004>.

Samaei, S.M., Gato-Trinidad, S., Altaee, A. (2018), "The

- application of pressure-driven ceramic membrane technology for the treatment of industrial wastewaters – A review”, *Sep. Purif. Technol.*, **200**, 198-220.
<https://doi.org/10.1016/j.seppur.2018.02.041>.
- Song, I.H., Bae, B.S., Ha, J.H., Lee, J. (2017), “Effect of hydraulic pressure on alumina coating on pore characteristics of flat-sheet ceramic membrane”, *Ceram. Int.*, **43**(13), 10502-10507.
<https://doi.org/10.1016/j.ceramint.2017.05.098>.
- Su, L., Hong, R., Kong, D., Wu, J. (2020), “Enhanced activity towards polyacrylates and poly(vinyl acetate) by site-directed mutagenesis of *Humicola insolens* cutinase”, *Int. J. Biol. Macromol.*, **162**, 1752-1759.
<https://doi.org/10.1016/j.ijbiomac.2020.07.261>.
- Wang, J., Yu, W., Graham, N.J.D., Jiang, L. (2020), “Evaluation of a novel polyamide-polyethylenimine nanofiltration membrane for wastewater treatment: Removal of Cu^{2+} ions”, *Chem. Eng. J.*, **392**, 123769. <https://doi.org/10.1016/j.cej.2019.123769>

SP